AIP | Physics of Plasmas
#1 JOURNAL IN 2014 GOOGLE SCHOLAR METRICS FOR THE PLASMA & FUSION CATEGORY

Fast response of electron-scale turbulence to auxiliary heating cessation in National Spherical Torus Experiment

Y. Ren, W. X. Wang, B. P. LeBlanc, W. Guttenfelder, S. M. Kaye, S. Ethier, E. Mazzucato, K. C. Lee, C. W. Domier, R. Bell, D. R. Smith, and H. Yuh

Citation: Physics of Plasmas **22**, 110701 (2015); doi: 10.1063/1.4935113
View online: http://dx.doi.org/10.1063/1.4935113
View Table of Contents: http://scitation.aip.org/content/aip/journal/pop/22/11?ver=pdfcov
Published by the AIP Publishing

Articles you may be interested in

Experimental study of parametric dependence of electron-scale turbulence in a spherical tokamaka)
Phys. Plasmas **19**, 056125 (2012); 10.1063/1.4719689

Suppressing electron turbulence and triggering internal transport barriers with reversed magnetic shear in the National Spherical Torus Experimenta)
Phys. Plasmas **19**, 056120 (2012); 10.1063/1.4718456

Multi-field/multi-scale turbulence response to electron cyclotron heating of DIII-D ohmic plasmas
Phys. Plasmas **18**, 082504 (2011); 10.1063/1.3610552

Resolving electron scale turbulence in spherical tokamaks with flow shear
Phys. Plasmas **18**, 022506 (2011); 10.1063/1.3551701

Role of nonlinear toroidal coupling in electron temperature gradient turbulencea)
Phys. Plasmas **12**, 056125 (2005); 10.1063/1.1894766

TREK
www.trekinc.com

HIGH-VOLTAGE AMPLIFIERS AND ELECTROSTATIC VOLTMETERS
ENABLING RESEARCH AND INNOVATION IN DIELECTRICS, MICROFLUIDICS, MATERIALS, PLASMAS AND PIEZOS

This article is copyrighted as indicated in the article. Reuse of AIP content is subject to the terms at: http://scitation.aip.org/termsconditions. Downloaded to IP: 66.180.182.80 On: Tue, 03 Nov 2015 18:54:23

Fast response of electron-scale turbulence to auxiliary heating cessation in National Spherical Torus Experiment

Y. Ren,[1] W. X. Wang,[1] B. P. LeBlanc,[1] W. Guttenfelder,[1] S. M. Kaye,[1] S. Ethier,[1] E. Mazzucato,[1] K. C. Lee,[2] C. W. Domier,[3] R. Bell,[1] D. R. Smith,[4] and H. Yuh[5]
[1]*Princeton Plasma Physics Laboratory, Princeton, New Jersey 08543, USA*
[2]*National Fusion Research Institute, Daejeon 305-806, South Korea*
[3]*University of California at Davis, Davis, California 95616, USA*
[4]*University of Wisconsin-Madison, Madison, Wisconsin 53706, USA*
[5]*Nova Photonics, Inc., Princeton, New Jersey 08540, USA*

(Received 13 December 2014; accepted 12 October 2015; published online 3 November 2015)

In this letter, we report the first observation of the fast response of electron-scale turbulence to auxiliary heating cessation in National Spherical Torus eXperiment [Ono *et al.*, Nucl. Fusion **40**, 557 (2000)]. The observation was made in a set of RF-heated L-mode plasmas with toroidal magnetic field of 0.55 T and plasma current of 300 kA. It is observed that electron-scale turbulence spectral power (measured with a high-k collective microwave scattering system) decreases significantly following fast cessation of RF heating that occurs in less than 200 μs. The large drop in the turbulence spectral power has a short time delay of about 1–2 ms relative to the RF cessation and happens on a time scale of 0.5–1 ms, much smaller than the energy confinement time of about 10 ms. Power balance analysis shows a factor of about 2 decrease in electron thermal diffusivity after the sudden drop of turbulence spectral power. Measured small changes in equilibrium profiles across the RF cessation are unlikely able to explain this sudden reduction in the measured turbulence and decrease in electron thermal transport, supported by local linear stability analysis and both local and global nonlinear gyrokinetic simulations. The observations imply that nonlocal flux-driven mechanism may be important for the observed turbulence and electron thermal transport. © *2015 AIP Publishing LLC*. [http://dx.doi.org/10.1063/1.4935113]

Understanding electron thermal transport is crucial for improving and predicting the confinement performance of future fusion devices, e.g., ITER and Fusion Nuclear Science Facility (FNSF).[1] Microturbulence is considered to be a major candidate in driving electron thermal transport in fusion plasmas.[2] One important way to study the relation between electron thermal transport and turbulence is to measure dynamic responses of plasma to a sudden external perturbation. For example, injecting impurity into tokamak edge plasmas was used to induce a sudden edge cooling in some early experiments,[3,4] where an almost simultaneous rise in core electron temperature was observed with respect to edge cooling. However, the measured core density fluctuation amplitude showed no obvious change responding to the improved electron thermal confinement in the core. Modulated Electron Cyclotron Heating (ECH) on Large Helical Device (LHD) was used to induce sudden change in electron heating in the core,[5,6] where low-k turbulence is observed to have much faster response to ECH modulation than the local Electron Temperature Gradient (ETG). These observations are used to show that the local turbulence may not be solely determined by local thermodynamic quantities and their gradients and that the observed electron thermal transport may be nonlocal. However, to the authors' knowledge, no observation of the response of electron-scale turbulence and electron thermal transport to a sudden change in auxiliary heating has been reported for spherical tokamaks (STs) operating in very different parameter regimes than conventional tokamaks.[7] We believe that such an observation in a ST is important for developing and validating theories and models for electron thermal transport. Furthermore, there is accumulated evidence that electron-scale (high-k) turbulence, i.e., ETG turbulence, can be important for driving anomalous electron thermal transport in tokamaks.[8–10] Thus, how electron-scale (high-k) turbulence behaves when subjected to external perturbations is of great interest to study.

Here, we present the first experimental observation of the fast response of electron-scale turbulence to auxiliary heating cessation in National Spherical Torus Experiment (NSTX).[11] The observations were made at the times of RF cessation in a set of NSTX RF-heated L-mode plasma with $B_T = 0.55$ T and $I_p = 300$ kA. Local electron-scale turbulence was measured with a 280 GHz collective microwave scattering system (the high-k scattering system) with a fine radial localization of ± 2 cm,[12] and the scattering system was configured to measure turbulence for a $k_\perp \rho_s$ ($k_\perp$ is the perpendicular wavenumber, and ρ_s is the ion gyroradius at electron temperature) range of about 2–10 at the radial region of $R \approx 133$–137 cm ($r/a \approx 0.57$–0.63, named as the high-k measurement region). We note that due to the tangential launching scheme employed,[12] the scattering system measures mostly radial wavenumber, k_r, and finite but smaller binormal wavenumber, k_θ, e.g., a range of $k_r \rho_s \sim 1.3$–9 and a range of $k_\theta \rho_s \sim 2$–3.5 for the experiments presented in this paper. The fine radial resolution of $\triangle R \approx \pm 2$ cm is the unique feature of the high-k scattering system, which is made possible by the tangential launching scheme together with the large toroidal curvature of NSTX.[13] This fine radial

 © 2015 AIP Publishing LLC

This article is copyrighted as indicated in the article. Reuse of AIP content is subject to the terms at: http://scitation.aip.org/termsconditions. Downloaded to IP: 66.180.182.80 On: Tue, 03 Nov 2015 18:54:23

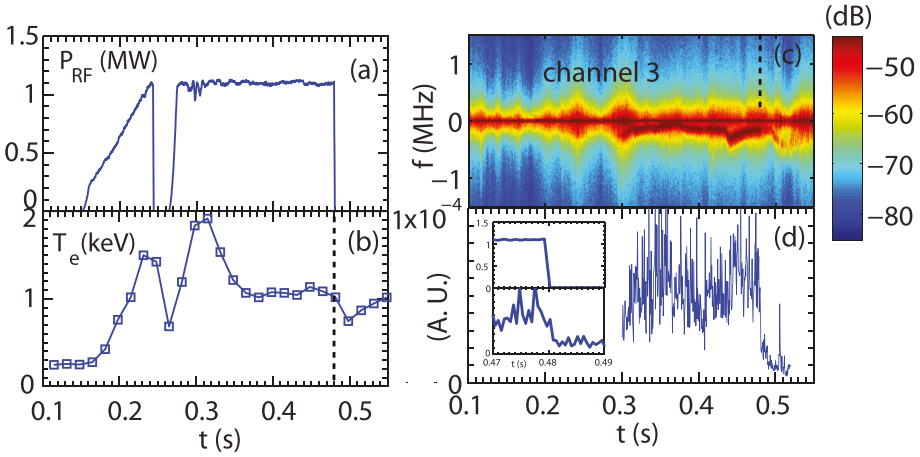

FIG. 1. The time traces of (a) injected RF power and (b) maximum T_e; (c) the spectrogram of the scattering channel 3 (measuring to a normalized wavenumber of about $k_\perp\rho_s \sim 4$–5); (d) time trace of the peak spectral power of the scattering signal. The inset in (d) shows the total injected RF power (upper panel) and the time trace of the peak spectral power of the scattering signal (lower panel) from t = 470 to 490 ms, where the large drop in the scattering signal following the RF cessation can be easily seen (RF heating is turned off in less than 200 μs). Black vertical dashed lines in (b) and (c) denote the time point at which the RF heating is terminated, i.e., t = 479.6 ms. Note that the time trace in (d) is only shown from $t = 300$ to 520 ms when the scattering signal, the spectral peaks at $f < 0$, can be clearly separated from the stray radiation, i.e., the central peak at $f = 0$.

resolution allows us to study the evolution of local fluctuation with respect to local equilibrium quantities and local heat flux from power balance analysis. In the rest of this letter, we will present results from a typical shot 140301 for which we have carried out extensive analysis.

The correlation between the cessation of RF heating and the reduction in electron-scale turbulence is demonstrated in Fig. 1. Figure 1(a) shows that the peak injected RF power is about 1 MW and the RF heating terminates at $t = 479.6$ ms (denoted by vertical dashed lines in Fig. 1). The maximum electron temperature, T_e, measured by a Thomson scattering system[14] is shown in Fig. 1(b), and it is clearly seen that the maximum T_e drops after RF heating terminates (the RF heating in NSTX provides core electron heating[15]). Figure 1(c) shows the spectrogram of the signal from channel 3 of the high-k scattering system, measuring to a normalized wavenumber of $k_\perp\rho_s \sim 4$–5. The scattering signal, i.e., the spectral peaks at $f < 0$ shown in Fig. 1(c), can be distinguished easily from the stray radiation, i.e., the central peak at $f = 0$, from about $t = 300$ ms to 550 ms, and we can see that a sudden drop in scattered signal power at almost the same time as the RF cessation at $t = 479.6$ ms. This sudden drop is more clearly shown in Fig. 1(d), where the time trace of the peak spectral power of the scattering signal in Fig. 1(c) is shown (the large drop in the scattering signal following the RF cessation can be easily seen). We note that the cessation of injected RF power is fast and occurs in less than 200 μs, which can be seen in the inset in Fig. 1(d). To establish a causal relation between the RF heating cessation and the reduction in measured turbulence, a careful examination of their temporal relation is as follows.

A closer examination of the temporal evolution of the measured high-k turbulence is shown in Fig. 2. Spectrogram of scattering channel 3 is shown in Fig. 2(a), and the local k spectra at $t = 479$ ms (green open square, before RF cessation), 484 ms (black asterisk, after RF cessation), and 492 ms (magenta open circle, after RF cessation) are shown in Fig. 2(b) with channel numbers denoted. Now, it is easy to determine the time of the sudden drop in turbulence spectral power from Fig. 2(a) to be about $t \approx 481$ ms. We also find that the drop in the spectral power happens approximately 1–2 ms after the RF cessation. The spectrogram also shows that the drop in turbulence occurs in about 0.5–1 ms, much smaller than the energy confinement time, about 10 ms, of these RF-heated L-mode plasmas. Thus, we would not expect that the observed fast reduction of turbulence spectral power is due to the change in equilibrium profiles, and we will further support this with gyrokinetic simulations shown in later in the paper. The propagation direction of measured turbulence is determined to be in the electron diamagnetic drift direction (not shown and see Refs. 16 and 17 for the method used). Thus, the observed turbulence has the

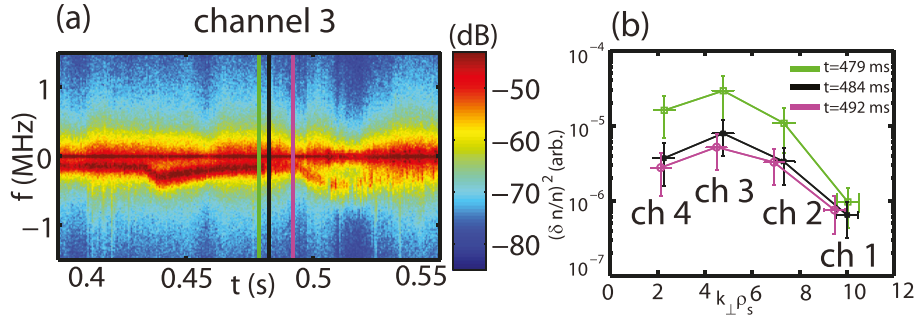

FIG. 2. (a) The spectrogram of scattering channel 3 around the time of RF cessation, $t = 479.6$ ms; (b) the local k spectra at $t = 479$ ms (green open square, before RF cessation), 484 (black asterisk, after RF cessation), and 492 ms (magenta open circle, after RF cessation). The three colored lines (a) denote time points used in (b) with the same color coding. Scattering channel numbers are denoted in (b).

This article is copyrighted as indicated in the article. Reuse of AIP content is subject to the terms at: http://scitation.aip.org/termsconditions. Downloaded to IP: 66.180.182.80 On: Tue, 03 Nov 2015 18:54:23

propagation direction consistent with ETG turbulence. We note that it is also possible that some of the measured electron-scale turbulence is driven by ITG/TEM modes through nonlinear coupling.[18,19] Indeed, ITG/TEM modes are unstable in the high-k measurement region. More quantitative evaluation of the drop in turbulence spectral power is shown in Fig. 2(b), which plots wavenumber spectra from four scattering channels (only four channels are used in the analysis since channel 5 measuring the smallest wavenumber was dominated by stray radiation and was partially blocked by the vacuum vessel). It can be seen that the wavenumber spectra at $t = 479$ ms (at about the RF cessation and before the sudden drop in spectral power seen in Fig. 2), 484 ms, and 492 ms (after the RF cessation and the sudden drop of turbulence) are shown (the wavenumber spectra was averaged over 3 ms around the denoted time points). Note that although after the RF cessation the turbulence spectral power varies little from t = 484 to 492 ms, the drop in the spectral power is up to about a factor of 7 from $t = 479$ ms (at the RF cessation) to 484/492 ms (after the RF cessation). We note that the drop seems to happen only at lower wavenumbers, namely, $k_\perp \rho_s \lesssim 9$, which suggests that the longer wavelength modes, $k_\perp \rho_s \lesssim 9$, may be more responsible for driving electron thermal transport.

Here, we present the equilibrium profile changes across the RF cessation. Figure 3(a) shows the electron temperature, T_e, profiles at t = 465, 482, and 498 ms measured the Thomson scattering system,[14] and Fig. 3(b) shows the ion temperature, T_i, profiles at $t = 436$ and 496 ms measured by charge exchange recombination spectroscopy (CHERS) measurements[20] with neutral beam blips (one blip from t = 430 to 445 ms and the second blip from t = 490 to 555 ms). It can be seen that the T_e profiles before (t = 465 ms) and right after the RF cessation (t = 482 ms) show small changes in the high-k measurement region (the shaded region) and T_i profiles only show small variation from $t = 436$ to 496 ms (although T_i measurements are noisier than the T_e measurements). Figures 3(c)–3(e) show the time evolution of some relevant equilibrium gradients averaged in the high-k measuring region at three exact time points of Thomson scattering measurements ($t = 465$, 482, and 498 ms) across the RF cessation. In particular, only small temporal variations ($\lesssim 15\%$) from $t = 465$ ms to 498 ms are seen for the normalized density, T_e and T_i gradients [a/L_{n_e} (c), a/L_{T_e} (d) and a/L_{T_i} (e)] (variation in other equilibrium quantities is similar). We note that the second Thomson time point, $t = 482$ ms, is after the RF cessation and also right after the sudden drop in measured turbulence at $t \approx 481$ ms. We emphasize that although the first Thomson time point, $t = 465$ ms, is separated by 17 ms from the second Thomson time point, $t = 482$ ms, the gradient variation between the two time points seen in Fig. 3 is still small. This strongly suggests that the equilibrium profiles at $t = 465$ ms may be able to represent the profiles right before the RF cessation. Furthermore, the 15% variation in the equilibrium gradients over 17 ms (from 465 to 482 ms) also strongly suggests that the variation in gradients on the 0.5–1 ms time scale should be $\lesssim 15\%$. We also note that taken into account of the confinement time of about 10 ms, the variation in gradients on the 0.5–1 ms time scale could be much less than 15%.

Electron thermal transport was evaluated with TRANSP transport analysis code[21] coupled with TORIC calculation for the RF heating profile.[22] The amount of RF power coupled into the plasma is estimated by evaluating the peak increasing rate of total stored energy at the RF turn-on phase (from t = 265 to 300 ms), and it shows that approximately

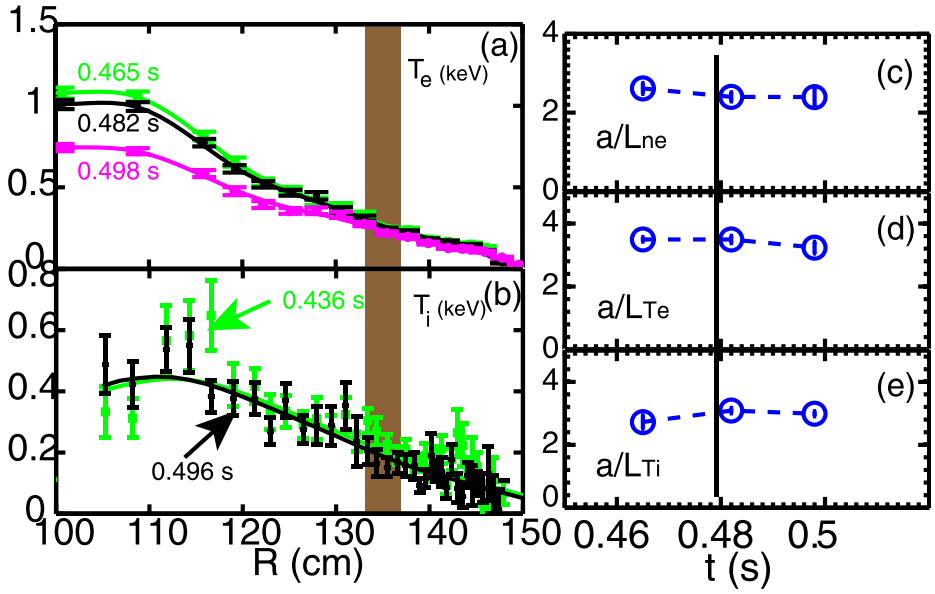

FIG. 3. (a) Radial profiles of electron temperature at t = 465, 482, and 498 ms; (b) radial profiles of ion temperature at t = 436 and 496 ms. The shaded regions in (a) and (b) denote the measuring region of the high-k scattering system. (c)–(e): Three equilibrium quantities averaged in the high-k measuring region at three exact Thomson measurement time points ($t = 465$, 482, and 498 ms). The error bars denote the spatial variation of these equilibrium quantities in the high-k measurement region. The error in a/L_{T_e} from the Thomson measurement is about 15%. The vertical solid line in (c), (d), and (e) denotes the time of the RF cessation. Note that all gradients are normalized to a, the half width of last closed flux surface at mid-plane. Note that the ion gradients in (e) at the Thomson time point are calculated from the nearest CHERS measurement time points.

This article is copyrighted as indicated in the article. Reuse of AIP content is subject to the terms at: http://scitation.aip.org/termsconditions. Downloaded to IP: 66.180.182.80 On: Tue, 03 Nov 2015 18:54:23

30% of the total RF power is coupled into the plasma. This estimation assumes that thermal transport does not change significantly in the RF turn-on phase, and this assumption is partly supported by the fact that no significant scattering signal is seen from t = 265 to 300 ms [see Fig. 1(c)]. The electron thermal diffusivity, χ_e, profiles at two exact Thomson measurement time points ($t = 465$ and 482 ms) as used in Fig. 3 are shown in Fig. 4, where a factor of 2 decrease in χ_e can be seen after the RF cessation at $t = 482$ ms. We note that such a drop in χ_e is correlated with the sudden drop in electron-scale turbulence spectral power shown in Fig. 2(b) but not correlated with the variations in the local equilibrium gradients as we have shown in Fig. 3.

Linear stability analysis using the GS2 gyrokinetic code[23] has been performed to explore instabilities operating in the high-k measurement region in these RF-heated L-mode plasmas with local Miller equilibrium,[24] electromagnetic effects, electron and ion collisions, and carbon impurity. While ITG/TEM and ETG modes are found to be unstable, the linear growth rates of these modes do not change significantly enough before and after RF cessation (not shown) to be able to explain observed the sudden drop in the turbulence spectral power seen in Fig. 2, consistent with our expectation from the fact that equilibrium profiles do not change significantly before and after the RF cessation (see Fig. 3). Local gyrokinetic simulations have also been used to assess profile stiffness since turbulence can be sensitive to small changes in gradients if it is close to marginal stability. The linear critical a/L_{T_e} and a/L_{T_i} for the ITG/TEM and ETG modes are assessed using the GS2 code. It is found that with a reduction in either a/L_{T_e} or a/L_{T_i} by a factor of 2, the linear growth rates remain large (0.25–0.5 C_s/a). Thus, the modes are far from marginal stability. As for the ETG modes, we found that the critical inverse electron temperature gradient scale length, $a/L_{T_e,crit}$, is 2.1, about 40% lower than the experimental a/L_{T_e} of 3.6. Compared with the $\lesssim$15% change in gradient before and after the RF cessation, these results show that the ion-scale and electron-scale modes are all far from marginal stability and are robustly unstable before and right after the RF cessation in these plasmas. Thus, we conclude that the linear stability framework is unlikely able to explain the observed reduction in electron-scale turbulence at the RF cessation. We have carried out gradient-driven nonlinear local gyrokinetic simulations using GYRO code[25] for both ion scale and electron scale,[30] and the results show that the electron temperature profile is far from stiff; e.g., a 25% increase in electron temperature gradient only leads to an 18% increase in electron energy flux from the ion-scale simulations, and the experimental electron temperature gradient is also far away from nonlinear threshold. We note that the predicted electron thermal transport from these nonlinear simulations do not match experimental value well, i.e., significantly under-predicted for the electron-scale simulations and significantly over-predicted for the ion-scale simulations. However, this is hardly surprising since the experimental observations indicate that local transport model may not be sufficient.

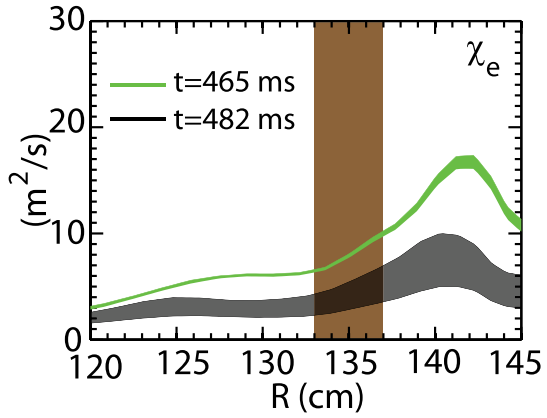

FIG. 4. Electron thermal diffusivity, χ_e, at t = 465 ms (about 14 ms before RF cessation) and 482 ms (after RF cessation) plotted as colored bands with vertical width denoting standard deviation. The rectangular shaded region denotes the measurement region of the high-k scattering system.

Here, we would like to emphasize that we have gone beyond local theory to explore global effects which may be able to explain the experimental observation since the equilibrium profile changes outside of the high-k measurement region may affect turbulence and thus electron thermal transport in the high-k measurement region, e.g., from turbulence spreading.[26] Ion-scale global nonlinear gyrokinetic simulations are carried out with the particle-in-cell Gyrokinetic Tokamak Simulation (GTS) code[27] for $t = 465$ ms (before the RF cessation) and for $t = 482$ (after the RF cessation) with experimental equilibrium profiles to assess effects from profile variation on electron thermal transport in the high-k measurement region. These global simulations cover a radial domain from $\Psi_N = 0.25$ to 0.8 ($R \sim 120$ cm to 147 cm) with buffer regions at $\Psi_N < 0.35$ and $\Psi_N > 0.7$ ($R < 127$ cm and $R > 144.5$ cm), where Ψ_N is the square root of the normalized toroidal flux. The size of grids on poloidal planes is about local ρ_i, and 80 particles per cell · species are used (with kinetic electrons and collisions; no impurity species included). The experimental equilibrium $E \times B$ shear is turned-on from the beginning of the simulations. Figure 5 compares electron energy flux, $Q_{e,GTS}$, radial profiles at $t = 465$ and 482 ms from GTS simulations with experimental electron heat flux, $Q_{e,exp}$ at the same two time points. It can be clearly seen in Fig. 5 that while $Q_{e,GTS}$ is essentially the same for both $t = 465$ ms (before the RF cessation) and for $t = 482$ ms (after the RF cessation) at $R \gtrsim 136$ cm, $Q_{e,GTS}$ at $R \lesssim 134$ cm is larger at $t = 482$ ms (after the RF cessation) than at $t = 465$ ms (before the RF cessation). We emphasize that the observed change in $Q_{e,GTS}$ before and after the RF cessation is opposite to the change in electron heat flux, $Q_{e,exp}$, before ($t = 465$ ms) and after ($t = 482$ ms) the RF cessation from power balance analysis as shown in Fig. 5, i.e., $Q_{e,exp}$ at $t = 465$ ms (before the RF cessation) is about a factor of 2 higher than $Q_{e,exp}$ $t = 482$ ms (after the RF cessation). On the other hand, the GTS simulation result is consistent with our expectation from local linear stability analysis described above. Thus, we conclude that global effects from profile variation, e.g., turbulence spreading, are not likely able to explain the observed reduction in electron thermal transport after the RF cessation and also the reduction in electron-scale turbulence if we consider the possible

This article is copyrighted as indicated in the article. Reuse of AIP content is subject to the terms at: http://scitation.aip.org/termsconditions. Downloaded to IP: 66.180.182.80 On: Tue, 03 Nov 2015 18:54:23

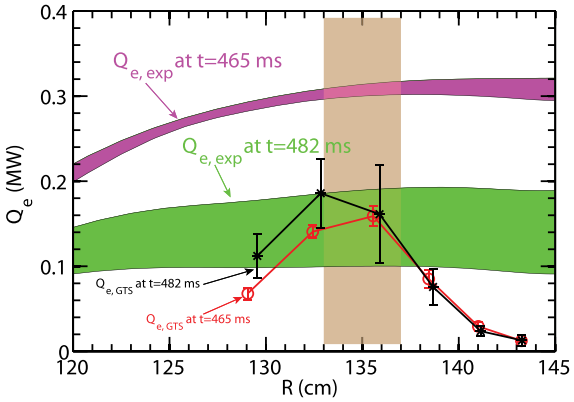

FIG. 5. Red circles: electron energy flux, $Q_{e,GTS}$, at $t = 465$ ms (before the RF cessation) as a function of major radius from nonlinear GTS simulation (averaged over a quasi-steady saturation period); black asterisks: $Q_{e,GTS}$ at $t = 482$ ms (after the RF cessation) from nonlinear GTS simulation (averaged over a quasi-steady saturation period); magenta band: experimental $Q_{e,exp}$, radial profile at $t = 465$ ms from experiment power balance analysis; green band: $Q_{e,exp}$ radial profile at $t = 482$ ms from experiment power balance analysis. Note that the vertical widths of the magenta and green bands denote the experimental uncertainties. The error bars of Q_e from nonlinear GTS simulations are the standard deviation of Q_e in the quasi-steady saturation periods of the simulations. The width of dashed rectangle denotes the high-k measurement region, i.e., from $R = 133$ to 137 cm. We note that the large difference between $Q_{e,GTS}$ and $Q_{e,exp}$ at $R > 140$ cm is probably due to a buffer region at $R > 144.5$ cm.

nonlinear interaction between ion-scale and electrons-scale turbulence as suggested in Refs. 18 and 19. We also note that $Q_{e,GTS}$ at $t = 465$ and 482 ms are both in good agreement with $Q_{e,exp}$ at $t = 482$ ms (after the RF cessation) but not with $Q_{e,exp}$ at $t = 465$ ms (before the RF cessation). This shows that even global nonlinear gyrokinetic simulations, taken into account not only the temporal variation but also the spatial variation of the equilibrium profiles before and after the RF cessation, may not explain the observed drop in electron thermal transport and turbulence. Finally, we would like to conclude that gradient-driven simulations either local or global seem not be able to explain experimental observations.

In summary, we present the first experimental observation of fast response of electron-scale turbulence to auxiliary heating cessation in a set of NSTX RF-heated L-mode plasmas. The results clearly show a time delay of about 1–2 ms between the RF cessation and the drop in measured electron-scale turbulence, indicating a causal relation between the two. The drop in turbulence spectral power happens on a 0.5–1 ms time scale, much smaller than the energy confinement time of abut 10 ms. The measured equilibrium quantities before and after the RF cessation are estimated to vary $\lesssim$15%, probably much less than 15% over the 0.5–1 ms time scale of the turbulence drop since the energy confinement time is much larger. Power balance analysis shows a factor of about 2 decrease in electron thermal diffusivity after the sudden drop of measured turbulence. Linear analysis using experimental profiles show that the change in linear growth rates from equilibrium variations fails to provide a consistent explanation of the experimental observations and local nonlinear gyrokinetic simulations also fail to provide an explanation. More importantly, our global nonlinear gyrokinetic simulations with actual experimental profiles before and after the RF cessation using GTS code[27] also failed to reproduce the reduction in turbulence and transport after the RF cessation (this takes into account all the equilibrium changes occurred, not just the electron temperature gradient). Thus, fixed-gradient models based on the changes in local/global equilibrium profiles across the RF cessation seem to be insufficient to explain the observed fast drop in turbulence and electron thermal transport after the RF cessation. However, we would like to note that the observation may be intuitively consistent with a picture of flux-driven turbulence: a decrease in heat flux leads to a decrease in turbulence responsible for thermal transport. A recent theoretical work has provided a nice foundation for the flux-driven turbulence.[28] We note that there are also other possible explanations for the observed fast response in turbulence to the RF cessation, e.g., effects of possible non-Maxwellian distributions due to RF heating[29] (although the RF cessation occurs on a time scale less than 200 μs as mentioned before, the non-Maxwellian effects due to the RF heating could persist on an ion collisional time scale and last longer than 200 μs) and electron-scale turbulence and the cross-scale coupling between ion- and electron-scale turbulence.

The authors would like to thank the NSTX team for the excellent technical support for this work. This work was supported by the U.S. Department of Energy under Contract Nos. DE-AC02-76CH03073, DE-FG03-95ER54295, and DE-FG03-99ER54518. Nonlinear simulations were carried out at the National Energy Research Scientific Computing Center.

[1]J. E. Menard, L. Bromberg, T. Brown, T. Burgess, D. Dix, L. El-Guebaly, T. Gerrity, R. J. Goldston, R. J. Hawryluk, R. Kastner *et al.*, Nucl. Fusion **51**, 103014 (2011).
[2]W. Tang, Nucl. Fusion **18**, 1089 (1978).
[3]M. Kissick, E. Fredrickson, J. Callen, C. Bush, Z. Chang, P. Efthimion, R. Hulse, D. Mansfield, H. Park, J. Schivell *et al.*, Nucl. Fusion **34**, 349 (1994).
[4]K. W. Gentle, W. L. Rowan, R. V. Bravenec, G. Cima, T. P. Crowley, H. Gasquet, G. A. Hallock, J. Heard, A. Ouroua, P. E. Phillips *et al.*, Phys. Rev. Lett. **74**, 3620 (1995).
[5]S. Inagaki, T. Tokuzawa, T. Kobayashi, S.-I. Itoh, K. Itoh, K. Ida, A. Fujisawa, S. Kubo, T. Shimozuma, N. Tamura *et al.*, Nucl. Fusion **54**, 114014 (2014).
[6]K. Ida, Z. Shi, H. Sun, S. Inagaki, K. Kamiya, J. Rice, N. Tamura, P. Diamond, G. Dif-Pradalier, X. Zou *et al.*, Nucl. Fusion **55**, 013022 (2015).
[7]S. M. Kaye, F. M. Levinton, D. Stutman, K. Tritz, H. Yuh, M. G. Bell, R. E. Bell, C. W. Domier, D. Gates, W. Horton *et al.*, Nucl. Fusion **47**, 499 (2007).
[8]W. Dorland, F. Jenko, M. Kotschenreuther, and B. N. Rogers, Phys. Rev. Lett. **85**, 5579 (2000).
[9]Y. Ren, S. M. Kaye, E. Mazzucato, W. Guttenfelder, R. E. Bell, C. W. Domier, B. P. LeBlanc, K. C. Lee, N. C. Luhmann, D. R. Smith *et al.*, Phys. Rev. Lett. **106**, 165005 (2011).
[10]W. Guttenfelder and J. Candy, Phys. Plasmas **18**, 022506 (2011).
[11]M. Ono, S. Kaye, Y.-K. Peng, G. Barnes, W. Blanchard, M. Carter, J. Chrzanowski, L. Dudek, R. Ewig, D. Gates *et al.*, Nucl. Fusion **40**, 557 (2000).
[12]D. R. Smith, E. Mazzucato, W. Lee, H. K. Park, C. W. Domier, and N. C. Luhmann, Rev. Sci. Instrum. **79**, 123501 (2008).
[13]E. Mazzucato, Phys. Plasmas **10**, 753 (2003).
[14]B. P. LeBlanc, R. E. Bell, D. W. Johnson, D. E. Hoffman, D. C. Long, and R. W. Palladino, Rev. Sci. Instrum. **74**, 1659 (2003).

This article is copyrighted as indicated in the article. Reuse of AIP content is subject to the terms at: http://scitation.aip.org/termsconditions. Downloaded to IP: 66.180.182.80 On: Tue, 03 Nov 2015 18:54:23

[15]B. LeBlanc, R. Bell, S. Kaye, D. Stutman, M. Bell, M. Bitter, C. Bourdelle, D. Gates, R. Maingi, S. Medley *et al*., Nucl. Fusion **44**, 513 (2004).
[16]E. Mazzucato, R. Bell, S. Ethier, J. Hosea, S. Kaye, B. LeBlanc, W. Lee, P. Ryan, D. Smith, W. Wang *et al*., Nucl. Fusion **49**, 055001 (2009).
[17]Y. Ren, W. Guttenfelder, S. M. Kaye, E. Mazzucato, R. E. Bell, A. Diallo, C. W. Domier, B. P. LeBlanc, K. C. Lee, D. R. Smith *et al*., Phys. Plasmas **19**, 056125 (2012).
[18]F. Jenko, J. Plasma Fusion Res. Series **6**, 11 (2004).
[19]Y. Ren, W. Guttenfelder, S. Kaye, E. Mazzucato, R. Bell, A. Diallo, C. Domier, B. LeBlanc, K. Lee, M. Podesta *et al*., Nucl. Fusion **53**, 083007 (2013).
[20]R. E. Bell, Rev. Sci. Instrum. **77**, 10E902 (2006).
[21]R. J. Hawryluk, *Physics of Plasma Close to Thermonuclear Conditions* (Pergamon, New York, 1981).
[22]M. Brambilla, Plasma Phys. Controlled Fusion **44**, 2423 (2002).
[23]M. Kotschenreuther, G. Rewoldt, and W. Tang, Comput. Phys. Commun. **88**, 128 (1995).
[24]R. L. Miller, M. S. Chu, J. M. Greene, Y. R. Lin-Liu, and R. E. Waltz, Phys. Plasmas **5**, 973 (1998).
[25]J. Candy and R. E. Waltz, Phys. Rev. Lett. **91**, 045001 (2003).
[26]W. X. Wang, T. S. Hahm, W. W. Lee, G. Rewoldt, J. Manickam, and W. M. Tang, Phys. Plasmas **14**, 072306 (2007).
[27]W. X. Wang, P. H. Diamond, T. S. Hahm, S. Ethier, G. Rewoldt, and W. M. Tang, Phys. Plasmas **17**, 072511 (2010).
[28]S.-I. Itoh and K. Itoh, Sci. Rep. **2**, 860 (2012).
[29]T. M. Biewer, R. E. Bell, S. J. Diem, C. K. Phillips, J. R. Wilson, and P. M. Ryan, Phys. Plasmas **12**, 056108 (2005).
[30]These simulations are with carbon impurities, electromagnetic effects, and collisions; $k_\theta\rho_s = 0.148$–2.23 and $k_\theta\rho_s = 1.6$–73 for the ion-scale and electron-scale simulations, respectively.

This article is copyrighted as indicated in the article. Reuse of AIP content is subject to the terms at: http://scitation.aip.org/termsconditions. Downloaded to IP: 66.180.182.80 On: Tue, 03 Nov 2015 18:54:23